REPORT DOCUMENTATION PAGE

Form Approved
OMB No. 0704-0188

1. REPORT DATE (DD-MM-YYYY) 24-02-2010	2. REPORT TYPE Journal Article	3. DATES COVERED (From - To)

4. TITLE AND SUBTITLE

Faraday Probe Analysis, Part 2: Evaluation of Facility Effects on Ion Migration in a Hall Thruster Plume (Preprint)

5a. CONTRACT NUMBER

5b. GRANT NUMBER

5c. PROGRAM ELEMENT NUMBER

6. AUTHOR(S)

Daniel L. Brown (AFRL/RZSS); Alec D. Gallimore (University of Michigan)

5d. PROJECT NUMBER

5e. TASK NUMBER

5f. WORK UNIT NUMBER
33SP0708

7. PERFORMING ORGANIZATION NAME(S) AND ADDRESS(ES)

Air Force Research Laboratory (AFMC)
AFRL/RZSS
1 Ara Road
Edwards AFB CA 93524-7013

8. PERFORMING ORGANIZATION REPORT NUMBER

AFRL-RZ-ED-JA-2010-064

9. SPONSORING / MONITORING AGENCY NAME(S) AND ADDRESS(ES)

Air Force Research Laboratory (AFMC)
AFRL/RZS
5 Pollux Drive
Edwards AFB CA 93524-7048

10. SPONSOR/MONITOR'S ACRONYM(S)

11. SPONSOR/MONITOR'S NUMBER(S)
AFRL-RZ-ED-JA-2010-064

12. DISTRIBUTION / AVAILABILITY STATEMENT

Approved for public release; distribution unlimited (PA #10101).

13. SUPPLEMENTARY NOTES
For publication in the Review of Scientific Instruments.

14. ABSTRACT

A nested Faraday probe was designed and fabricated to assess facility effects in a systematic study of ion migration in a Hall thruster plume. Current density distributions were studied at 8, 12, 16, and 20 thruster diameters downstream of the Hall thruster exit plane with four probe configurations at background pressures of 3x10-6, 1x10-5, and 3x10-5 torr. Several correction factors are applied to account for the effective probe collection area and systematic measurement error associated with measuring an annular device as an axisymmetric point source. These corrections enable the investigation of facility effects on beam expansion and ion migration in the plume. The effects of background facility neutrals are isolated, which enables precise and accurate estimate of thruster ion beam current and plume divergence. A set of guidelines are recommended for Faraday probe design, experimental approach, and data analysis of results that are aimed at minimizing measurement error of far-field Faraday probe measurements. These guidelines are shown to reduce the calculated ion beam current by 10-20% compared to conventional analysis techniques and to reduce measurement uncertainty to approximately ±3%. The reductions in measurement uncertainty and the increased capability to approximate the onorbit plume expansion from ground-based measurements are a significant improvement for comparisons with numerical simulations and investigations of Hall thruster performance.

15. SUBJECT TERMS

16. SECURITY CLASSIFICATION OF:			17. LIMITATION OF ABSTRACT	18. NUMBER OF PAGES	19a. NAME OF RESPONSIBLE PERSON Dr. William A. Hargus, Jr.
a. REPORT Unclassified	b. ABSTRACT Unclassified	c. THIS PAGE Unclassified	SAR	38	19b. TELEPHONE NUMBER (include area code) N/A

Standard Form 298 (Rev. 8-98)
Prescribed by ANSI Std. 239.18

Faraday Probe Analysis, Part 2: Evaluation of Facility Effects on Ion Migration in a Hall Thruster Plume (Preprint)

Daniel L. Brown
Spacecraft Branch, Propulsion Directorate
Air Force Research Laboratory, Edwards AFB, CA 93524

and

Alec D. Gallimore
Plasmadynamics and Electric Propulsion Laboratory, Department of Aerospace Engineering,
The University of Michigan, Ann Arbor, MI, 48109

A nested Faraday probe was designed and fabricated to assess facility effects in a systematic study of ion migration in a Hall thruster plume. Current density distributions were studied at 8, 12, 16, and 20 thruster diameters downstream of the Hall thruster exit plane with four probe configurations at background pressures of 3×10^{-6}, 1×10^{-5}, and 3×10^{-5} torr. Several correction factors are applied to account for the effective probe collection area and systematic measurement error associated with measuring an annular device as an axisymmetric point source. These corrections enable the investigation of facility effects on beam expansion and ion migration in the plume. The effects of background facility neutrals are isolated, which enables precise and accurate estimate of thruster ion beam current and plume divergence. A set of guidelines are recommended for Faraday probe design, experimental approach, and data analysis of results that are aimed at minimizing measurement error of far-field Faraday probe measurements. These guidelines are shown to reduce the calculated ion beam current by 10-20% compared to conventional analysis techniques and to reduce measurement uncertainty to approximately ±3%. The reductions in measurement uncertainty and the increased capability to approximate the on-orbit plume expansion from ground-based measurements are a significant improvement for comparisons with numerical simulations and investigations of Hall thruster performance.

I. INTRODUCTION

The advantages of Hall effect thruster (HET) technology for in-space maneuvers and interplanetary trajectories are due to high efficiency operation and high thrust density at moderate specific impulse in the range of 1000 to 3000 seconds. Hall thrusters operate through the plasmadynamic interactions of applied electromagnetic fields with injected propellant and electrons from an external cathode. Knowledge of the ion current density profile in the exhaust beam may be used to quantify dominant performance loss mechanisms associated with plume divergence, the ionization mass fraction, and electron current to the anode. Faraday probes have been used to quantify these characteristics in numerous laboratory investigations, but have a high degree of uncertainty attributed to facility effects.

The facility effects inherent in ground-based Hall thruster investigations manifest in two ways. The first is ionization and subsequent acceleration of facility neutral particles near the discharge exit, which results in a population low velocity, highly divergent ions that increases the thruster discharge current, thrust, and measured ion current density in the plume. The second interaction arises through charge exchange (CEX) collisional processes between ions generated in the thruster discharge channel with background facility neutral particles, which results in particle scattering events that increase current density on the periphery of the plume. These facility interactions have been investigated by many groups with several Hall thruster designs, all of which found that facility effects escalate at high background pressure, and may alter the thruster performance and plume properties [1,2,3].

A number of investigations have studied nude Faraday probe design modifications to minimize the collection of these low energy ions generated through facility effects. Filtering mechanisms have been investigated to mitigate the collection of low energy ions in electric

propulsion plumes. One approach is to attach a collimator to the entrance of a nude Faraday probe to filter disperse, low energy ions that are created by CEX collisions in the plume [3,4].

Further efforts utilized a magnetic field to filter low energy CEX ions. A study by Rovey [5] compared results from a magnetically filtered Faraday probe, a boxed Faraday probe, and a nude Faraday probe to separately assess the effect of the magnetic filter and the boxed collimator that houses the filter. The magnetically filtered and boxed Faraday probes resulted in decreased ion beam current and diminished current density on the periphery compared to the nude Faraday probe. These findings indicate the boxed collimator and magnetic filtering decrease low energy CEX ions collected by the Faraday probe. The disadvantage of collimator and filtering configurations are that they do not selectively isolate facility effects from the ionization of thruster and cathode neutrals downstream of the primary acceleration zone. A collimated Faraday probe collects both the low energy thruster ion population and CEX facility ions created near the thruster exit, whereas the magnetically filtered Faraday probe does not collect either population. Therefore, neither diagnostic captures the true on-orbit plume characteristic of an electric propulsion system.

Several analytical methods have been developed to account for collection of low energy facility CEX ions in the periphery of the plume. Nevertheless, the integrated ion beam current from far-field measurements is typically larger than the value reported from near-field measurements, and is often greater than the thruster discharge current. Analytical techniques include subtracting the ion current density at the periphery of the plume ($\theta=0°$) from the entire beam profile, or extrapolating the exponential region ($30°<\theta<60°$) of the ion current density to the outer periphery ($0°<\theta<30°$). While these approaches provide a simple alternative to the experimental methods or probe design modifications, they are limited in determining the spatial

influence of facility effects throughout the plume. Subtracting a finite current density from the profile is based on the assumption that probe collection of ambient tank ions is uniform throughout the plume. The exponential extrapolation technique is based on the spatial decay of beam ions on the edges of the primary beam, but removes features of the outer periphery that may arise due to CEX collisions near the thruster exit. Neither of these techniques accurately captures the angular distribution of low energy ions that would be present on orbit.

To further study the over-prediction of integrated ion beam current, plasma potential in the region surrounding a nude Faraday probe has been measured to study the possibility of probe bias voltage acting as a point source potential sink, and thereby attracting low energy CEX ions [6]. Langmuir probe measurements near a nude Faraday probe resulted in potential variations less than 3-V within 20-mm of the probe. It was concluded that CEX ions had a negligible attraction to the probe bias potential, and the random flux of low energy ions was insufficient to explain the increased current density at high background pressure and large off-axis angles. This conclusion was consistent with a hybrid-PIC model of the ion flow around an axisymmetric Faraday probe, which concluded ion collection errors due to sheath expansion were minimal [7].

A different method for discerning CEX processes in the plume was demonstrated by de Grys [3] and more recently by Azziz [8], who compared Faraday probe measurements at individual locations in the plume at several background pressures and extrapolated the current density to vacuum conditions. This approach is a more advanced technique to experimentally assess CEX facility effects throughout the plume, and enables a more accurate estimation of the on-orbit ion current density profiles.

Despite extensive study of experimental methods and analytical techniques, Faraday probe measurements continue to be complicated by facility effects. This paper is Part 2 of a two-

part investigation designed to increase accuracy and systematically evaluate the measurement uncertainty of Faraday probe current density measurements associated with (1) probe design and (2) facility effects. A nested Faraday probe was developed and evaluated in Part 1 [9] to assess the effect of probe design and geometry on the ion collection area. The study identified ion current collection by the side-wall of the collector, which increased the calculated current density when the cross-sectional collector area is used. A correction factor was proposed to adjust the effective probe collection area for ions collected by the walls in the gap volume, which decreased the ion current density by 10% to 20% and resulted in values of integrated ion beam current consistent with expected values based on Hall thruster performance analyses [9]. Results from Part 1 of the investigation are applied to all measurements in this study of facility effects and ion migration.

In this paper, the effects of vacuum test facilities on measurements of collected ion current in the plume of a low-power Hall thruster are characterized by adjusting facility background pressure and measurement distance from the thruster exit plane. Facility effects due to background neutral gas are evaluated using methods analogous to de Grys [3] and Azziz [8]. This method is evaluated with four nested Faraday probe configurations, and is considered an accurate method to isolate facility effects and ascertain the influence on a Hall thruster plume. When combined with the results from Part 1, it enables experimental study of ion migration characteristics for comparison with simulations of the on-orbit plume. Due to the large spatial region surveyed in this investigation, an analytical study of systematic measurement error associated with evaluating the plume of annular thruster geometry with a spherical measurement coordinate system is included.

The primary aim of this paper is to develop a method for determination of systematic measurement error and facility effects in order to increase accuracy and reduce Faraday probe measurement uncertainty. Findings from the two-part investigation are unified to generate an outline of recommendations for Faraday probe design, experimental methods, and analysis of results in Section V. These guidelines are believed to reduce measurement uncertainty to approximately ±3%, which is significant improvement over the estimated ±20% or greater that is commonly reported.

II. EXPERIMENTAL APPARATUS

A. Vacuum Facility and Hall Thruster Ion Source

The evaluation of facility effects and ion migration was conducted in Chamber 1 at AFRL. Chamber 1 is a stainless steel, cylindrical vacuum chamber 2.3-m in diameter and 4-m in length. A schematic is shown in Fig. 1. A low-power laboratory Hall thruster was located along the centerline of the chamber and fired towards the cryopanels at the opposing end. All surfaces optically visible to the plasma plume were shielded with graphite felt. An Edwards DryStar GV160 mechanical booster pump reached rough vacuum and lighter gases were removed with a Varian TV55 turbomolecular pump. Two CVi TorrMaster cryotubs circulated liquid nitrogen to cool 4 cryopanels, and achieved a maximum xenon pumping speed of 50,000 l/s.

An MKS Instruments HPS Series cold cathode ionization gauge (CCG) was located on the chamber ceiling above the thruster centerline approximately 1 meter downstream of the exit plane. Facility background pressure p was calculated using Eq. (1):

$$p = \frac{p_i - p_b}{2.87} + p_b \,, \tag{1}$$

where p_i is the pressure measured by the ionization gauge and p_b is the base pressure of air, which was conservatively estimated at $p_b \approx 1 \times 10^{-7}$ torr. Chamber background pressure was increased by injecting xenon through an auxiliary flow line located approximately 1-meter downstream of the thruster exit plane. Injected flow of approximately 9, 29, and 127-sccm corresponded to a corrected xenon background pressure of 3.2×10^{-6}, 1.1×10^{-5}, and 3.5×10^{-5} torr, respectively. According to MKS Instruments, the CCG measurement reproducibility is within 5% of reading at constant temperature [10]. Uncertainty of the CCG is estimated at ±20%.
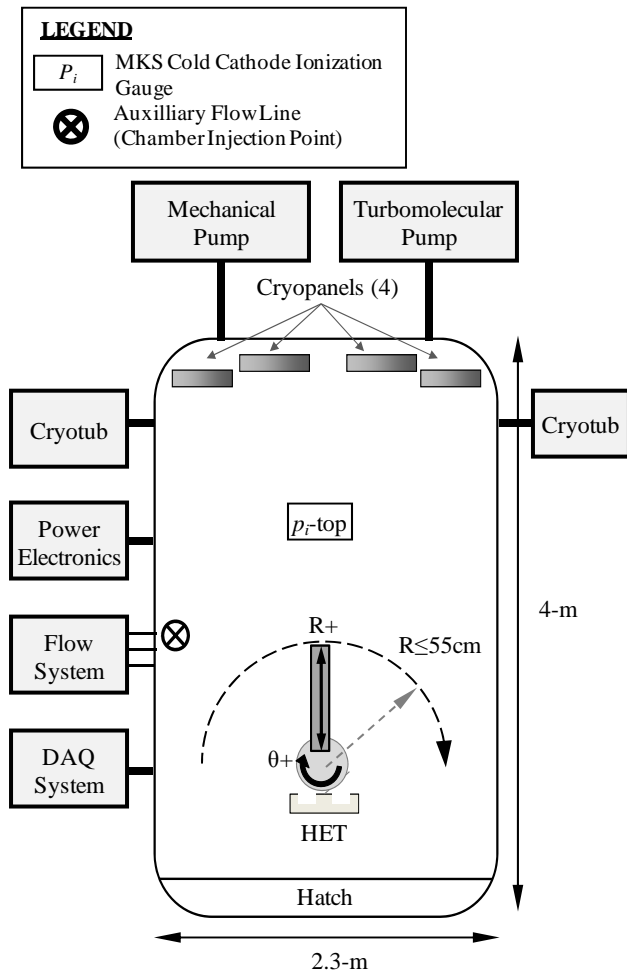

FIG. 1. Schematic of Chamber 1 at AFRL (not to scale).

The diagnostic (R,θ) positioning system consisted of a translation stage for control of measurement radius and a rotation stage, which was centered beneath the exit plane on thruster centerline. One end of the translation stage is mounted on top of the rotation stage, enabling current density scans from 0° to 180° at constant radius from the axis of rotation at the exit plane. These far-field measurements were taken in 2° increments for a spherical coordinate geometry. The Faraday probe and thruster were mounted approximately 50-cm above the rotation and translation stages. The overall uncertainty in measurement position is estimated at ±0.5 cm.

B. Nested Faraday Probe

A nested Faraday probe with two concentric collector rings and an outer guard ring was utilized in this investigation to enable simultaneous measurements of ion current density in the Hall thruster plume with the inner and outer collector. Two versions of the outer collector were machined to create a gap of either 0.5-mm or 1.5-mm between the rings. The diagnostic is shown in Fig. 2 in the 0.5-mm gap configuration.

FIG. 2. Photograph of the AFRL nested Faraday probe shown in the 0.5-mm gap width configuration.

Collected ion current was measured with both versions of the outer collector, which resulted in four probe collection geometries that may be studied using the nested Faraday probe. These configurations are defined as:

1. Configuration 1 – Current to the inner collector with a 0.5 mm gap

2. Configuration 2 – Combined current to the inner and outer collectors with a 0.5 mm gap

3. Configuration 3 – Current to the inner collector with a 1.5 mm gap

4. Configuration 4 – Combined current to the inner and outer collectors with a 1.5 mm gap

Collected current was measured with an Agilent 34970A Data Acquisition/Switch Unit, as illustrated in Fig. 3. An Agilent E3631A Triple Output DC power supply was used to bias the collectors and guard ring. The nested Faraday probe operation was characterized with variations in probe bias potential over a range of angular positions and downstream distances at several facility background pressures. A bias potential of -20 V with respect to facility ground was beyond the ion current saturation limit in all cases, and was used for all Faraday probe measurements.

The nested Faraday probe collectors were machined from arc-cast low-carbon grade-365 molybdenum, and the guard ring is grade-360 molybdenum. Differences in secondary electron emission (SEE) between the collectors and guard ring should be negligible. A boron nitride shell surrounds the guard ring, and stainless steel housing encloses the probe. This housing is attached to chamber ground. Additional details on the facility, diagnostics, and experimental methods can be found in Part 1 of this two-part study [9].
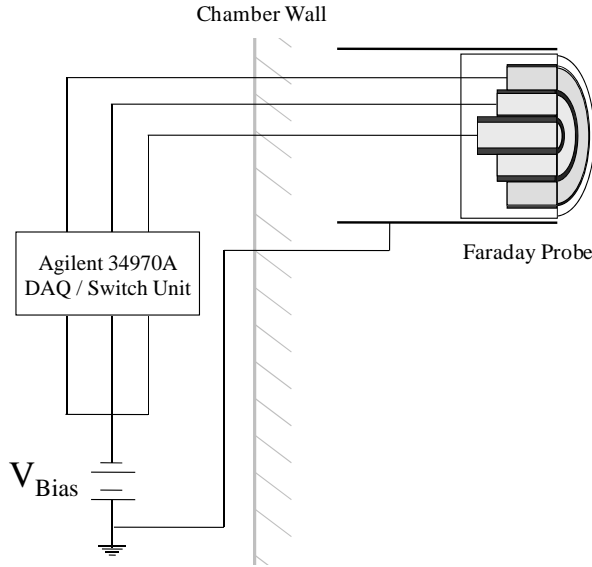
FIG. 3. Electrical diagram of the nested Faraday probe power electronics and DAQ system.

III. ANALYSIS OF SYSTEMATIC ERROR

A theoretical examination of the measurement coordinate system is necessary to isolate systematic trends due to facility effects in experimental measurements. The analysis is aimed at resolving the error caused by probe measurements with respect to a point source as opposed to the annular discharge geometry of a typical HET. In this analysis of systematic error, the thruster is modeled as two point ion sources located at the centerline of the discharge channel. Figure 4 illustrates the probe distance R and angular location θ with respect to the thruster centerline.

Two geometric corrections are analyzed. The first correction accounts for variations in probe angle with respect to the point sources, which will affect the current collection area. In a single point source analysis, where the ion point source is located at the probe axis of rotation, the probe face is perpendicular to the source as it is swept in a 180° arc. Modeling the thruster as two point sources changes this probe orientation, and the probe face is only perpendicular to the

point sources at 0° and 180°. The ion angle of incidence to the probe face changes with angular position and distance, and decreases the effective probe collection area of beam ions. In addition, the ion angle of incidence at a given location is different for each point source. The angles of incidence are calculated for the left and right point sources as α_L and α_R, and are used to evaluate cosine losses in the probe collection area.
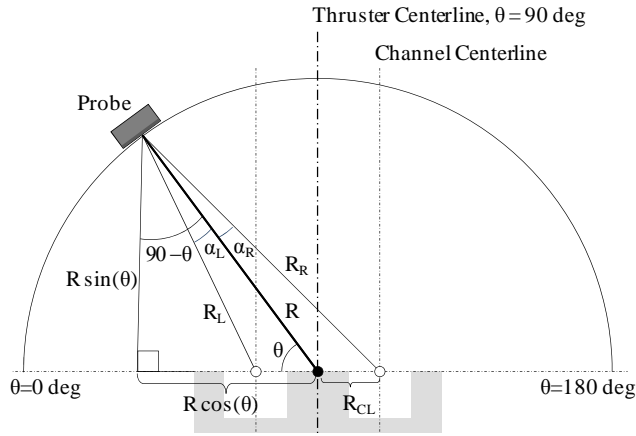

FIG. 4. Measurement coordinate system showing probe distance and angular location in a two-point source model.

The angles α_L and α_R are found using basic trigonometry and are formulated in Eq. (2) based on the geometry shown in Fig. 4. These effects are expressed in a generalized form based on θ, R, and the channel centerline radius R_{CL}. The ratio of R/R_{CL} is incorporated to simplify the analysis and enable a more direct comparison between large and small thrusters.

$$\alpha_{L,R}[\theta, R, R_{CL}] = \pm\left(90-\theta - \tan^{-1}\left(\frac{\cos(\theta)\mp\dfrac{R_{CL}}{R}}{\sin(\theta)}\right)\right) \qquad (2)$$

The probe collection area is corrected for cosine losses with the area correction factor, κ_A, using the average of α_L and α_R in Eq. (3).

$$\kappa_A[\theta, R, R_{CL}] = \cos^2\left(\frac{\alpha_L + \alpha_R}{2}\right) \tag{3}$$

The second correction accounts for differences in path length from the left and right point sources to the probe, which introduces systematic error in the R^2 term in the axisymmetric plume integration. The probe distances from the left and right point source are characterized as R_L and R_R. Similar to the analysis of ion angle of incidence, the path length will vary with probe angular position and is dissimilar for each point source. The exception is on thruster centerline, where the distance from the probe to each point source is equal and greater than the measurement radius of rotation, R.

The lengths R_L and R_R are calculated with respect to the measurement distance, R, in Eq. (4). The distance correction factor, κ_D, is defined in Eq. (5) as a function of θ, R, and R_{CL}.

$$\frac{R_{L,R}[\theta, R, R_{CL}]}{R} = \sqrt{(\sin(\theta))^2 + \left(\cos(\theta) \mp \frac{R_{CL}}{R}\right)^2} \tag{4}$$

$$\kappa_D[\theta, R, R_{CL}] = \left(\frac{1}{2}\left(\frac{R_L}{R} + \frac{R_R}{R}\right)\right)^2 \tag{5}$$

The effects of κ_D and κ_A are applied to all Faraday probe current density measurements, and the total ion beam current I_{Beam} is calculated using Eq. (6) for a Faraday probe scan at constant measurement radius R. This formulation incorporates the gap correction factor κ_G that was developed in Part 1 [9]. The gap correction factor is applied to the geometric probe collection area A_C to account for ions collected in the gap between the collector and guard ring.

$$I_{Beam} = 2\pi R^2 \int_0^{\pi/2} \frac{I[\theta, R]}{A_C + \kappa_G} \left(\frac{\kappa_D[\theta, R, R_{CL}]}{\kappa_A[\theta, R, R_{CL}]}\right) \sin(\theta) \, d\theta \tag{6}$$

where I[θ,R] is the ion current measured by a Faraday probe at angular position θ and radius R.

The spatial correction ratio (κ_D/κ_A) is displayed as a function of probe angular position in Fig. 5 for constant channel centerline diameters downstream (CCDD) of the diagnostic axis of rotation. The overall effect of this ratio is to increase current density in the plume central core, which ultimately increases the integrated ion beam current. Variation in collection area due to ion angle of incidence decreases rapidly with downstream distance, and the approximation of a point source measurement improves. In Fig. 6, the correction on thruster centerline is shown as a function of CCDD, calculated as $R/2R_{CL}$. The overall correction factor asymptotically approaches unity with downstream measurement distance, and is less than 1.01 for distances greater than 8 CCDD. Thus, including the spatial corrections minimizes a systematic source of error introduced from the hemispherical measurement system. All current density traces and beam current calculations in this investigation will incorporate the spatial corrections for ion angle of incidence and measurement distance using the formulation in Eq. (6).
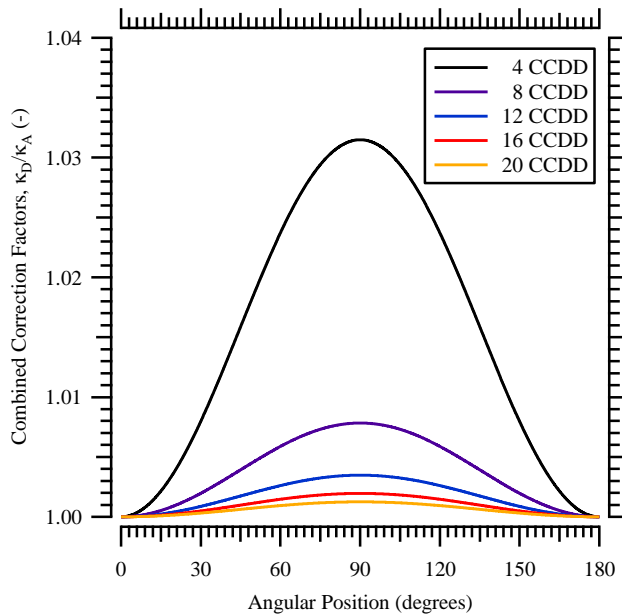

FIG. 5. Combined effect of the correction factors (κ_D/κ_A) accounting for the probe distance and angle with respect to the left and right ion point sources as a function of angular position with contours of constant $R/2R_{CL}$ = 4, 8, 12, 16, and 20 CCDD.
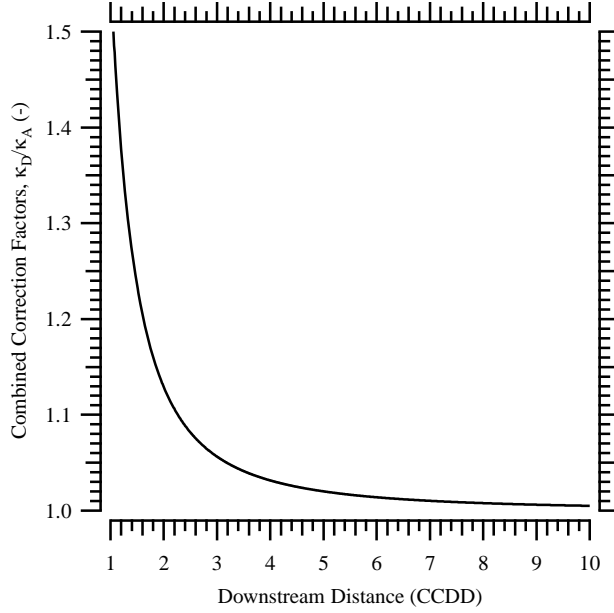
FIG. 6. Combined effect of the correction factors (κ_D/κ_A) on channel centerline (θ=90°) as a function of downstream thruster diameters ($R/2R_{CL}$).

The corrections in probe collection area are only valid for beam ions originating near the exit plane. Charge exchange collisions downstream of the primary ionization region increase dispersion of ion velocity, and the correction is not relevant to this population. In addition, the analysis does not account for channel width. This is of lesser concern, since minor variations in channel centerline radius will have a negligible effect on measurements taken beyond four thruster diameters.

IV. RESULTS

Far-field Faraday probe measurements are presumed to have relatively large uncertainty on the plume periphery due to facility effects. In this study, the ion current density at each angular location in the plume is characterized as a function of background pressure. Extrapolating the current density at discrete angular locations to vacuum conditions isolates effects arising from facility CEX ions and neutral ingestion. This technique is shown in Fig. 7

for Configuration 1 at 20 CCDD. Collected ion current is plotted in 10° increments as a function of facility background pressure. On thruster centerline at θ=90°, the collected current increased linearly with pressure. However, at ±10° from centerline the slope appears to transition and transforms to a slightly negative linear slope at ±20° and ±30° from thruster centerline. The reverse trend occurs at approximately ±40° and results in a positive linear slope on the periphery from ±60° to ±90° from thruster centerline.
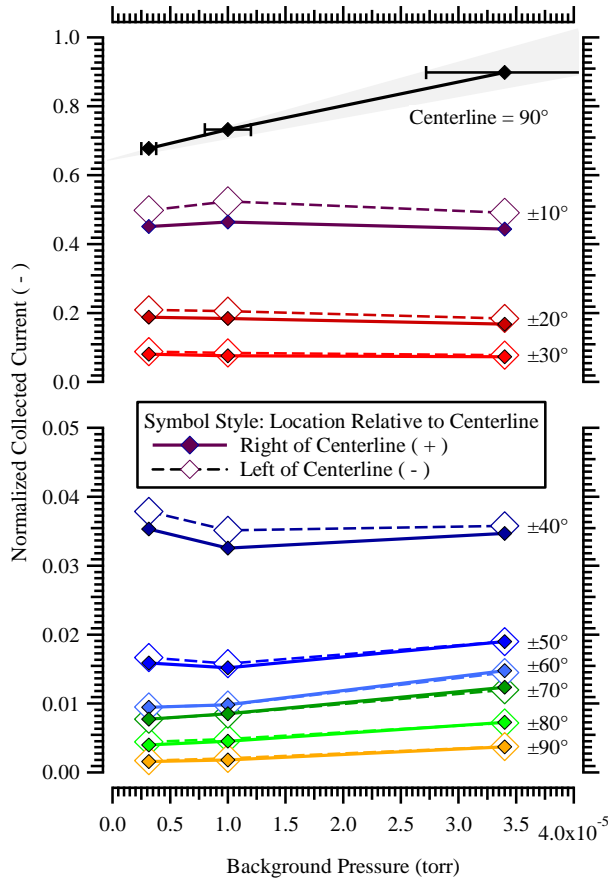

FIG. 7. Normalized collected ion current of Configuration 1 as a function of background pressure at discrete angular locations in the plume at 20 CCDD. Measurements are normalized to the maximum collected current of the profile at 3.4×10^{-5} torr.

A disadvantage of this technique is the uncertainty associated with determination of facility background pressure. This is due to both the measurement uncertainty of the CCG and the pressure gradients in the vacuum facility. A previous experimental investigation of the

pressure gradient in the 5-kW P5 HET plume found minimal variation approximately 1.5 meters downstream of the exit plane on centerline [11]. This distance is approximately 10 CCDD for the P5 (148-mm mean thruster diameter), which is comparable to the minimum distance of 8 CCDD in this investigation. As a consequence of this result, the facility background pressure gradient is expected to be minimal for all distances (8-20 CCDD).

The measurement uncertainty in CCG pressure readings is deemed to have a minor effect on the trends in Fig. 7. Although cold cathode ionization gauges are known to exhibit a non-linear relationship in the current-pressure characteristic, these attributes arise primarily at ultra high vacuum conditions and are attributed to gauge design, electrode operation, and field alignment [12]. The vacuum environment in this study ranges from $\sim 10^{-6}$ to $\sim 10^{-4}$ torr, where the CCG current-pressure characteristic has a higher degree of linearity [13]. Therefore, the CCG behavior is expected to be constant for all pressure measurements reported in this investigation. The $\pm 20\%$ uncertainty in the recorded pressure also has minimal effect on the slopes in Fig. 7, as illustrated by the shaded region surrounding the centerline data and 20% error bars. Although the centerline region has the largest slope and would be most affected by uncertainty in pressure, the extrapolation to vacuum conditions appears insensitive to this uncertainty.

These variations in the slope of the collected ion current with facility background pressure are plotted as a function of angular position in Fig. 8 at 8, 12, 16, and 20 CCDD. The transitions from positive to negative slope occur at approximately $\pm 10°$ from thruster centerline for all downstream distances. Similarly, the transition from negative to positive slope occurs at approximately $\pm 50°$ from thruster centerline for all downstream distances. Residuals show the degree of linearity at each angular location, and are calculated as the square of the Pearson product moment correlation coefficient. The residuals show that the transition at $\pm 50°$ moves

inwards toward the central core as downstream distance increases. This trend is indicative of the outward scattering of beam ions caused by CEX facility effects. Although increased background pressure increased the central core current density, the residuals indicate the angular location of ion migration from the central core within ±10° is largely unaffected by downstream distance.
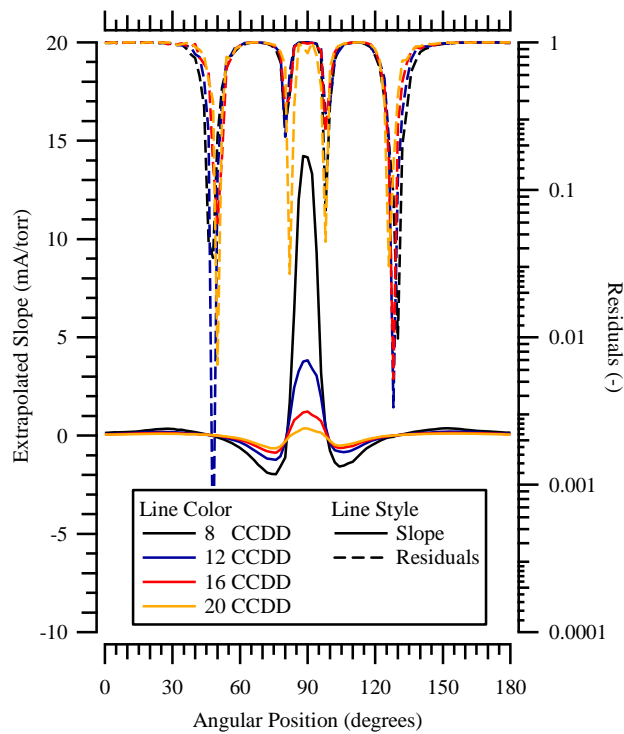

FIG. 8. Residuals and slope of the extrapolated collected ion current of the nested Faraday probe Configuration 1 as a function of angular position at 8, 12, 16, and 20 CCDD.

The slope of the extrapolated collected ion current density in Fig. 8 provides information about the angular location of increased current density due to neutral ingestion and dispersion from beam scattering due to CEX collisions with facility neutrals. The slope appears to be dominated by two distinct effects in the plume. These two effects are each modeled with a Gaussian distribution, and the modeled slope distribution is the superposition of these Gaussian best-fit curves. The choice of a Gaussian distribution is subjective, but may be appropriate for processes related to the thermal facility neutral propellant population. The two fitted Gaussian curves, the modeled slope, and the experimental slope are compared in Fig. 9 from 8 to 20

CCDD. The superposition of Gaussian distributions shows consistent agreement with the experimental distribution of slope for all downstream distances. Although the Gaussian distribution may not be the correct physical distribution, this analysis provides a qualitative characterization of the angular range and relative magnitude of facility effects in the plume.
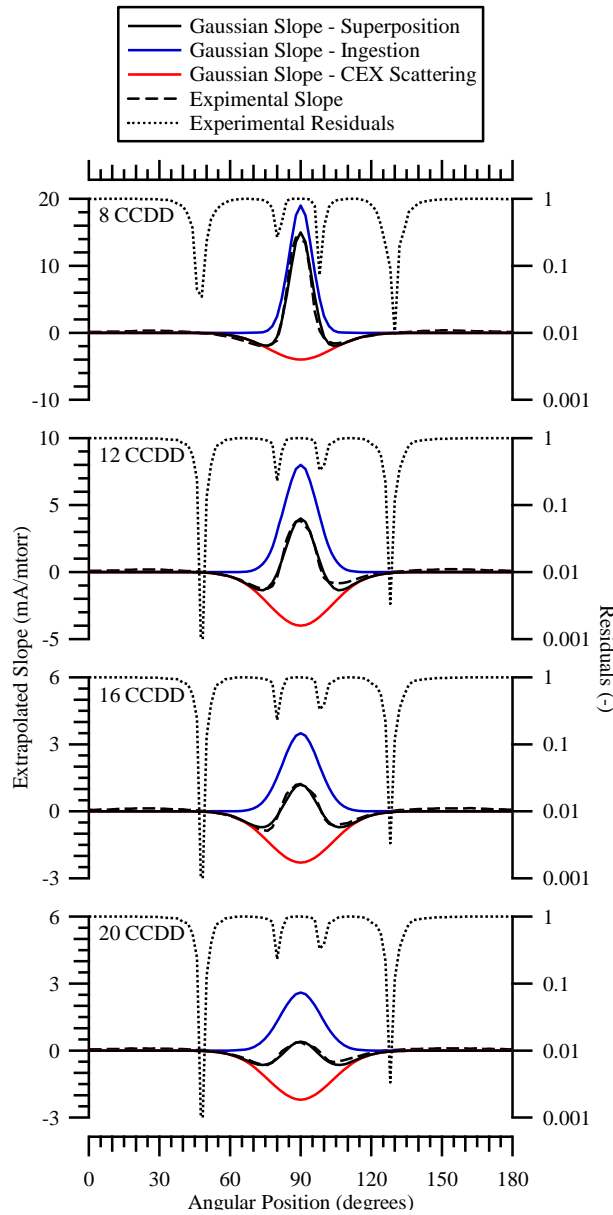

FIG. 9. Residuals and slope of the extrapolated collected ion current of the nested Faraday probe (Configuration 1) as a function of angular position at 8, 12, 16, and 20 CCDD. The experimental slope is compared to a superposition of two Gaussian curves at each downstream distance.

The first effect leads to a positive increase in the slope about thruster centerline, and is attributed to ionization and acceleration of ingested facility neutrals. The magnitude of the positive slope in the central core decreased with downstream distance as approximately R^2, and affected a slightly larger angular range of the plume as downstream distance increased. The decrease in slope is the result of expansion and CEX collisions with facility neutrals downstream of the primary acceleration zone, which results in further dispersion of the ion beam. The positive slope in the central core leads to a net increase in the integrated ion beam current, and corresponds to increased thrust and discharge current.

The second effect is broader and leads to a negative slope in the central core about thruster centerline. The slope is slightly positive beyond approximately $\pm 50°$ from thruster centerline for all downstream distances, and is the source of increased ion current density on the periphery of the plume at elevated facility background pressure. This effect is the result of CEX collisions with facility neutrals near the thruster exit downstream of the primary acceleration zone. In this case, no additional current is created and the ion beam is dispersed. The width of the Gaussian attributed to downstream CEX collisions with facility neutrals was relatively constant with downstream distance in the far-field plume.

The complete effects of background pressure on current density profiles are shown in Fig. 10. These profiles show the escalation of ion current density in the central core with background pressure, which was attributed to ionization of ingested neutrals upstream of the primary acceleration region. Increased current density on the periphery is primarily the result of ambient low energy facility ions and beam ion scattering from the central core due to CEX collisions.
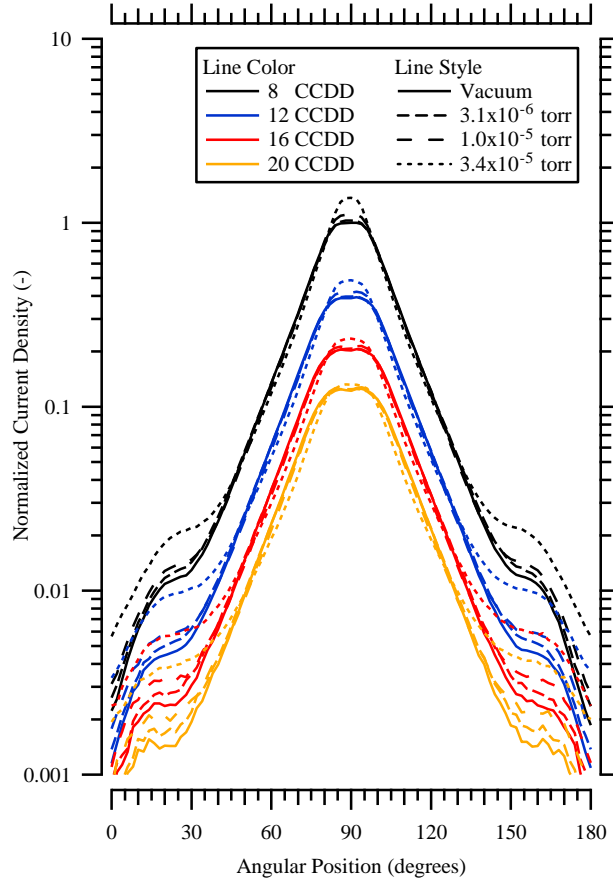
FIG. 10. Normalized ion current density profiles of the nested Faraday probe Configuration 1 as a function of angular position at 8, 12, 16, and 20 CCDD. The extrapolated vacuum profiles are compared to measurements at background pressures of 3.1×10^{-6}, 1.0×10^{-5}, and 3.4×10^{-5} torr. Current density profiles are normalized to the maximum extrapolated vacuum current density at 8 CCDD.

Current density profiles of the four nested Faraday probe configurations are extrapolated to vacuum conditions for all downstream distances in Fig. 11. These vacuum current density profiles isolate facility effects, and provide insight into the ion migration that would be present on-orbit. The configurations exhibit consistent profiles at all distances, and further increase confidence in the methods developed for determination of vacuum current density. The current density of Configuration 1 is slightly larger than the other configurations, and is attributed to measurement and/or alignment error of the inner collector. This increased current density profile manifests as a ~5% increase in the integrated ion beam current compared to the other configurations. The thruster current utilization efficiency, calculated as the ion beam current

relative to the total thruster discharge current I_d, is listed in Table I for vacuum conditions of all probe configurations at all downstream distances. Configurations 2, 3, and 4 are within a 0.03 range of current utilization for all downstream distances, and the magnitudes of ion beam current relative to discharge current are consistent with values expected from Hall thruster performance models [14].

TABLE I. Ratio of integrated ion beam current to thruster discharge current at vacuum conditions for nested Faraday probe Configurations 1 to 4 at 8, 12, 16, and 20 CCDD.

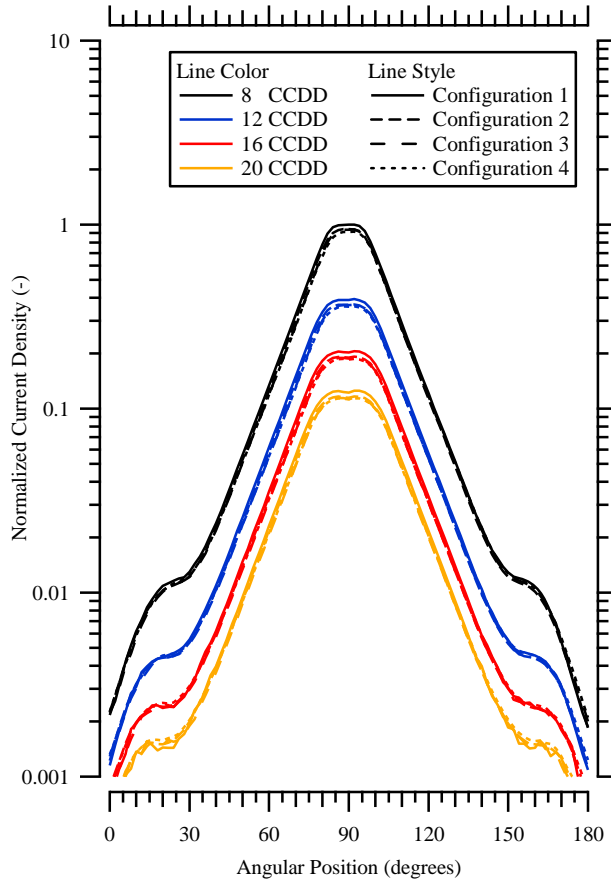| Downstream Distance [CCDD]	I_{Beam}/I_d			
	Configuration 1	Configuration 2	Configuration 3	Configuration 4
8	0.88	0.82	0.81	0.80
12	0.89	0.84	0.82	0.81
16	0.90	0.84	0.82	0.82
20	0.90	0.85	0.82	0.83

FIG. 11. Normalized ion current density profiles at vacuum conditions of the nested Faraday probe Configurations 1, 2, 3, and 4 as a function of angular position at 8, 12, 16, and 20 CCDD. Current density profiles are normalized to the maximum extrapolated vacuum current density of Configuration 1 at 8 CCDD.

V. DISCUSSION

A. Ion Migration in a Hall Thruster Plume

Elimination of beam scattering generated by facility effects enables the study of ion migration in the plume and enhances comparisons with numerical simulations. Figure 12 shows profiles of vacuum current density per unit solid angle at 8, 12, 16, and 20 CCDD. The residuals are shown to reveal the angular regions where the slope is approximately zero and background pressure has a minimal effect on the plume.
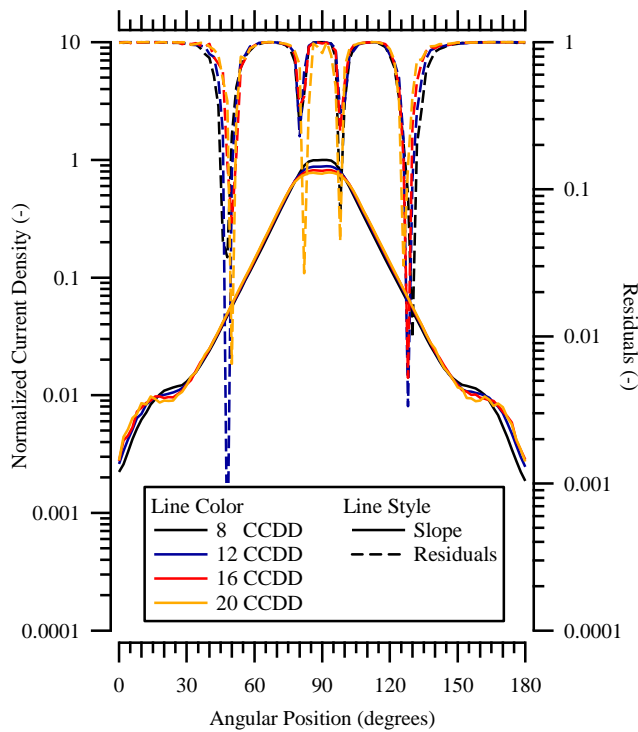

FIG. 12. Normalized profiles of ion current density per solid angle at vacuum conditions and residuals of the nested Faraday probe Configuration 1 as a function of angular position at 8, 12, 16, and 20 CCDD. Profiles are normalized to the maximum extrapolated vacuum current per steradian at 8 CCDD.

Total ion migration in the plume may be studied in greater detail using the angular distribution of ion beam current through the surface of a spherical stripe, as illustrated in Fig. 13. The angular distribution of ion beam current passing through a constant angular width stripe allows spatial analysis of beam current transport with distance and angle. Summing the ion

beam current passing through the stripes within a given half-angle results in the ion beam current per steradian, and the sum from θ=0° to 180° is the total ion beam current. The ion current passing through a stripe will be referred to in units of amperes per 1° degree wide stripe (A/ unit stripe).
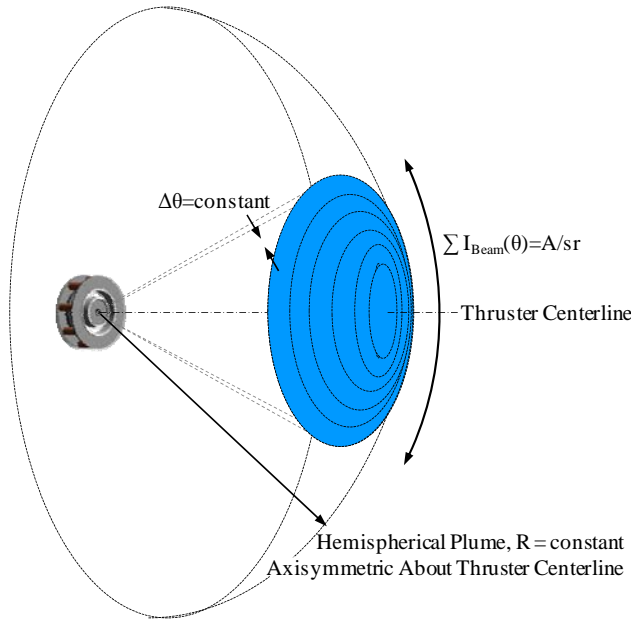

FIG. 13. Diagram of the axisymmetric spherical stripe coordinate geometry for analysis of angular ion beam current distribution in the plume.

The trends in Fig. 10 are examined as angular distributions of ion beam current in Fig. 14. The vacuum ion beam current per stripe is shown as a function of angular position for 8 CCDD. The upper plot in Fig. 14 shows the differences in vacuum ion beam current at 12, 16, and 20 CCDD relative to the vacuum ion beam current profile at 8 CCDD, calculated as I[θ,R]-I[θ,R=8 CCDD]. The lower plots show the difference in ion beam current at 3.1×10^{-6}, 1.0×10^{-5}, and 3.4×10^{-5} torr relative to the vacuum ion beam current profile at constant 8 CCDD, calculated as I[θ,p]- I[θ, *p=vacuum*]. .

Figure 14 highlights the significant impact facility effects have on the current density profiles relative to the vacuum conditions. Elevated facility background pressure amplified the

ion beam current on the periphery and increased ion beam current in the central core due to ingested facility neutrals. In this study, deviations from the vacuum beam current distribution reached 20% near the central core at 20 CCDD and the highest background pressure.

While facility pressure effects caused a large deviation in angular beam current profiles, the vacuum ion beam current profiles exhibit a lesser but consistent trend with downstream distance that warrants additional examination. The relative difference in the vacuum ion beam current was negligible at three angular locations in the plume for all downstream distances, not including the outer periphery at θ=0° and 180°. These angular locations of constant ion beam current corresponded to the zones where the residuals decreased and the extrapolated slope was zero in Fig. 8.
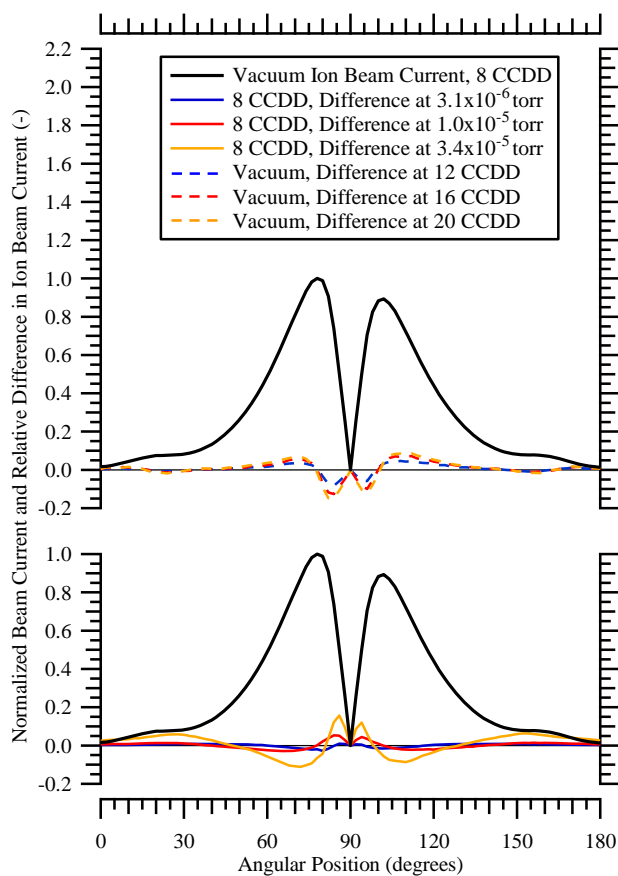

FIG. 14. Vacuum ion beam current per unit stripe at 8 CCDD compared to the difference in vacuum profiles with downstream distance (top) and to the difference at 8 CCDD with increasing background pressure (bottom). All profiles are normalized to the maximum extrapolated vacuum ion beam current at 8 CCDD.

The differences in vacuum ion beam current relative to the profile at 8 CCDD are further magnified in Fig. 15 from θ=0° to θ=90°. Regions of constant ion beam current in the plume are extremely consistent to within ±1°. These zones are located at θ=16°, θ=34°, and θ=78°. The relative difference in beam current per stripe at each downstream location is integrated as a function of angular position to evaluate the total transfer of beam current per steradian.
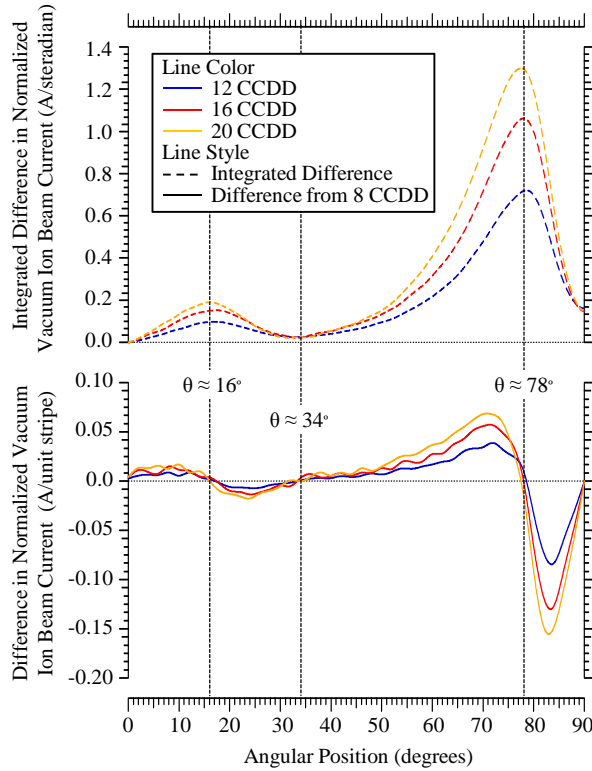

FIG. 15. Normalized difference in vacuum ion beam current (bottom) and the integral of the normalized difference (top) at 12, 16, and 20 CCDD relative to the profile at 8 CCDD as a function of angular position. Vacuum current density profiles are normalized to the maximum extrapolated vacuum beam current at 8 CCDD.

The upper plot in Fig. 15 reveals the overall transfer of ion beam current from 78° to 90° is transferred to the region between 34° and 78°. A negligible fraction of current migrates across the boundary at θ=34°, and suggests that the primary ion beam is approximately conserved within this angle for vacuum conditions at all downstream distances in the far-field plume. In a similar manner to the primary beam, the ion current from 16° to 34° is transferred to the region

between 0° and 16° at all downstream distances. The variation of integrated vacuum ion beam current in the plume from 0° to 180° varied by less than 2% from the value at 8 CCDD.

The experimental ion migration trends for vacuum conditions in Fig. 15 are compared to preliminary numerical simulations of the far-field plume using DRACO [15], an electrostatic Particle-In-Cell (PIC) module in COLISEUM [16,17]. DRACO uses a hybrid-PIC model of plasma processes with a kinetic description of heavy particles and a fluid description for the electrons. Collisions are modeled with Monte Carlo Collision (MCC) methods [18,19] in a Cartesian mesh framework. DRACO supports the standard finite-difference PIC method and utilizes a Boltzmann field solver based on the assumption that the potential is directly related to the charge density [20].

In these numerical simulations of the far-field plume, the ion source model is determined with a modified version of HPHall-2 using a three region mobility model [21]. HPHall-2 is an axisymmetric, hybrid fluid/PIC model of the Hall thruster discharge, where heavy particles are modeled with PIC methods [22] and electrons are modeled as a fluid [23].

In this comparison of ion migration, elastic processes and CEX collisions with the background gas were not included in COLISEUM simulations of the far-field plume, and therefore the numerical simulations will be compared to the experimental vacuum profiles. Two simulations of plume expansion were performed. The first simulation included CEX collisions with thruster neutrals. The second simulation did not incorporate CEX collisions in the plume. Comparisons of the experimental and simulated differences in vacuum ion beam current profiles relative to 8 CCDD are shown in Fig. 16. Differences in the potential field between the HPHall-2 ion source model and physical experiment are believed to be the cause of differences in the structure of ion migration.

Despite the differences in structure, the comparison of experimental and simulated results in Fig. 16 reveals important details about Hall thruster plume expansion in a vacuum. The simulation including CEX collisions with thruster neutrals exhibited minimal difference from the simulation without CEX processes. The simulated results matched the experimental regions of minimal ion migration near $\theta=34°$ and $\theta=78°$. In the absence of CEX collisions and elastic processes in the plume, the only source of ion migration is acceleration due to the external potential field structure. This indicates that far-field angular regions of constant vacuum ion beam current per stripe (centerline to $\theta=34°$) may arise due to minimal gradients in the external field, and far-field CEX collisions with thruster neutrals play a lesser role within this half-angle. In this case, the characteristics of ion migration in the far-field plume are captured with the COLISEUM model, despite probable differences in the near-field potential field between the source model and experiment. This outcome is attributed to negligible plasma potential gradients in the far-field plume compared to gradients in the near-field thruster plasma.

The simulation with thruster ion-neutral CEX collisions recreated features of the experimental structure between $\theta=0°$ and $\theta=34°$. The lack of structure within this region in the simulation without CEX collisions indicates this process is likely related to CEX collisions with thruster neutrals. The mechanisms that result in the overall plume structure are not fully understood, and require additional simulation and analysis.
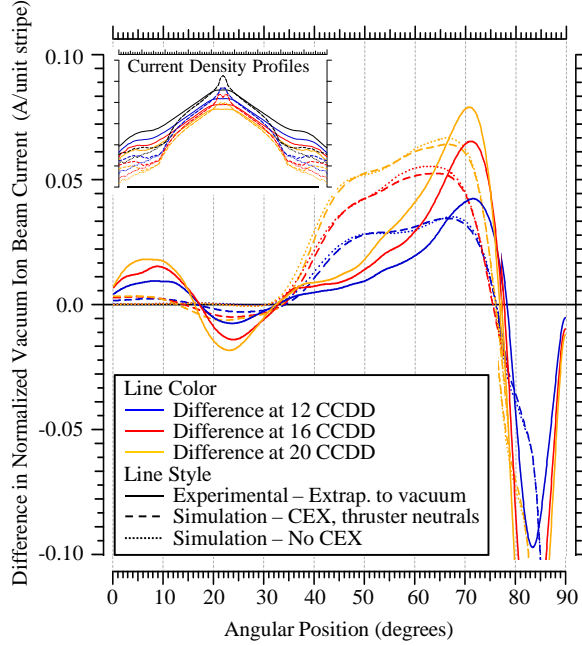
FIG. 16. Comparison of the simulated and experimental normalized differences in vacuum ion beam current at 12, 16, and 20 CCDD relative to the profile at 8 CCDD as a function of angular position. All profiles are normalized to the maximum extrapolated experimental vacuum beam current at 8 CCDD. The simulated and experimental normalized current density profiles are shown in the small window for reference.

B. Evaluation of Ion Beam Divergence

To accurately assess plume divergence, it is necessary to characterize the migration of primary beam ions in the plume due to external fields and CEX collisions with anode and cathode neutrals. Although this scattering would be present on-orbit, beam divergence downstream of the cathode neutralization plane will not diminish thrust. Therefore, accounting for this divergence will cause an over-prediction of plume divergence losses in the analysis of Hall thruster efficiency.

Jet momentum losses due to beam divergence are naturally expressed as a momentum-weighted average cosine [14]. Charge divergence in the plume is indicative of the loss in thrust due to off-axis ion velocity, and is often used as an alternative for experimental characterization of performance losses due to plume divergence. The momentum-weighted average cosine

$<\cos(\theta)>_{mv}$ is approximated as the charge-weighted average cosine $<\cos(\theta)>_J$ in Eq. (7) for an axisymmetric plume.

$$<\cos(\theta)>_{mv} \cong \frac{2\pi R^2 \int\limits_0^{\pi/2} I[\theta,R]\cos(\theta)\sin(\theta)\,d\theta}{2\pi R^2 \int\limits_0^{\pi/2} I[\theta,R]\,\sin(\theta)\,d\theta} =\ <\cos(\theta)>_J \tag{7}$$

An effective plume divergence angle, λ, may be calculated as shown in Eq. (8). This angle is significantly less than the 95% divergence half-angle that is typically reported for evaluation of plume expansion in electric propulsion thrusters.

$$\lambda = \cos^{-1}\left(<\cos(\theta)>_J\right) = \cos^{-1}\left(\frac{I_{Axial}}{I_{Beam}}\right) \tag{8}$$

The axial component of ion beam current is studied relative to the angle from channel centerline, as opposed to the conventional reference of thruster centerline. Figure 17 illustrates the reduction in plume divergence half-angle with respect to channel centerline, α_A, compared to the plume divergence angle with respect to thruster centerline, $90°\text{-}\theta$. The reference frame based on channel centerline reduces systematic error in plume divergence associated with beam ions in the central core, and is similar to the methodology developed in Section III to reduce the systematic error of a point source measurement coordinate system. The axial component of ion beam current I_{Axial} is calculated in Eq. (9) with respect to channel centerline using α_A.

$$I_{Axial} = 2\pi R^2 \int\limits_0^{\pi/2} \frac{I\left[\theta,R\right]\cos\left(\alpha_A[\theta,R,R_{CL}]\right)}{A_C + \kappa_G}\left(\frac{\kappa_D[\theta,R,R_{CL}]}{\kappa_A[\theta,R,R_{CL}]}\right)\sin(\theta)\,d\theta \tag{9}$$

In Fig. 17, the cosine loss in beam current is fixed at $\alpha_A = 0°$ in the central core and calculated with respect to channel centerline in the region beyond the central core to $\theta = 90°$. This piecewise function for α_A is expressed in Eq. (10).

$$\alpha_A\left[\theta, R, R_{CL}\right] = \begin{cases} \tan^{-1}\left(\dfrac{\cos(\theta) - \dfrac{R_{CL}}{R}}{\sin(\theta)}\right) & \text{for} \quad 0° \leq \theta \leq \cos^{-1}\left(\dfrac{R_{CL}}{R}\right) \\[4ex] 0 & \text{for} \quad \cos^{-1}\left(\dfrac{R_{CL}}{R}\right) \leq \theta \leq 90° \end{cases} \tag{10}$$
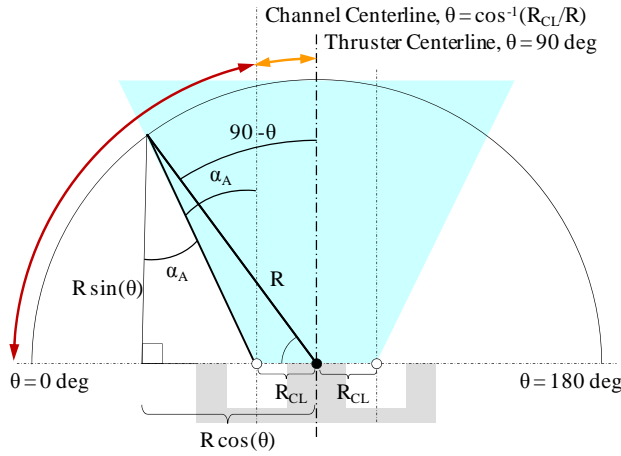

FIG. 17. Diagram of the axial component of beam current relative to channel centerline.

The ratio of the axial component of ion beam current calculated in Eq. (9) relative to the total ion beam current determined from Eq. (6) is shown for all background pressures and all configurations of the nested Faraday probe in Fig. 18. As downstream distance increases, the ratio decreases for all cases. This effect is expected and is primarily attributed to divergence caused by the external potential field structure, CEX collisions with anode and cathode neutrals, and CEX collisions with facility neutrals for the profiles at finite background pressure.
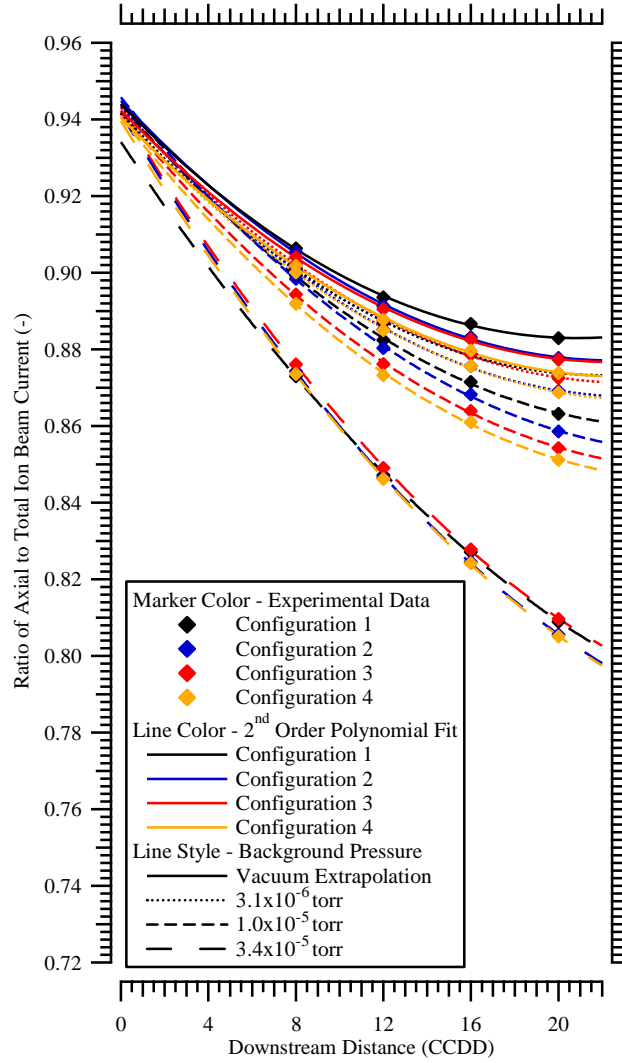
FIG. 18. Experimental data (markers) and 2nd order polynomial trendlines (lines) of the ratio of the axial component of ion beam current relative to the total ion beam current of the nested Faraday probe Configurations 1, 2, 3, and 4 as a function of downstream distance at background pressures of 3.1x10^{-6} torr, 1.0x10^{-5} torr, 3.4x10^{-5} torr, and the ratio extrapolated to vacuum. Experimental data deviates from the trendlines by less than ±0.1%.

It should be noted that the ratio of I_{Axial}/I_{Beam} extrapolated to vacuum conditions showed a significant decline with downstream distance, albeit less than the reduction with increased facility background pressure. This reveals that a significant source of plume divergence is unrelated to facility effects. Based on these measurements, the ratio of I_{Axial}/I_{Beam} may diminish by more than 5% in the near-field plume before reaching a steady value in the far-field plume.

This divergence occurs predominantly beyond the cathode neutralization plane, and will have a negligible affect the directed thrust or performance.

The coefficients of the 2nd order polynomial trendlines varied with background pressure. No universal function was found that correlated these coefficients to background pressure, discharge voltage, and mass flow rate. For a general 2nd order polynomial expression of the form $y(x)=A_2x^2+A_1x+A_0$, increased background pressure increased the coefficient A_1 and decreased the coefficient A_2. In this form, the coefficient A_0 is the ratio I_{Axial}/I_{Beam} at vacuum conditions.

Variations in the polynomial coefficients with discharge voltage and anode mass flow rate are more difficult to isolate and quantify due to the dependence on plume focusing and the location of ionization. Initial results indicate higher thruster discharge voltage decreased the magnitude of both coefficients. This relationship is attributed to the more collimated beam that is typically seen during high-voltage operation.

The anode mass flow rate is believed to have two competing effects on divergence. Increased propellant flow rate corresponds to a narrower axial region of ionization and acceleration in the discharge, along with a more concentrated ion density near channel centerline [24]. These effects lead to a decrease in divergence due to enhanced plume focusing, and would likely have a similar effect as discharge voltage on the polynomial coefficients. However, the increased neutral flow may also lead to increased CEX collisions with thruster neutrals downstream of the exit plane, thereby increasing ion scattering in the far-field plume. A simple analytical model is deemed insufficient to fully characterize the influence of beam focusing and facility effects on plume divergence. Additional systematic investigations and numerical simulations with a high fidelity source model are required to determine these relationships.

VI. RECOMMENDATIONS FOR HIGH ACCURACY FARADAY PROBE CURRENT DENSITY MEASUREMENTS

Based on the experimental results in this investigation, the recommended approach for high accuracy current density profiles is to characterize the plume with variations in facility background pressure and downstream distance. The analytical methods and experimental techniques described in this paper may be used to determine Hall thruster current density profiles and integrated ion beam current to a high degree of accuracy. In order to minimize uncertainty of far-field Faraday probe measurements, the following guidelines are recommended for Faraday probe design, experimental approach, and analysis of results. Several of these guidelines are conventional practice or have been recommended in previous literature [2,4,8].

1. Select a Faraday probe design with a 5 to 10 Debye length gap for a wide range of downstream distances and pressures. Select collector and guard ring material with minimal SEE coefficient, such as molybdenum, graphite, or tungsten [2].

2. Conduct Faraday probe current density measurements at a minimum of 3 facility background pressures to determine the vacuum current density profiles. The background pressures should range by at least one order of magnitude.

3. Conduct Faraday probe current density measurements at a minimum of 3 downstream distances to determine the axial component of ion beam current at the exit plane. For far-field measurements about a single axis of rotation using a spherical measurement coordinate system, the distance should be greater than 8 CCDD. For near-field measurements based on a cylindrical measurement coordinate system, spatial effects and cosine losses should be estimated and the maximum distance should be less than approximately one thruster diameter downstream using a dynamic window integration method [24] or similar technique.

4. Include the correction factors κ_A, κ_D and α_A to account for the use of a point source measurement coordinate system geometry for an annular thruster device.

5. Account for ions collected in the gap volume by increasing the effective ion collection area with κ_G. See Part 1 of this investigation for further explanation and implementation of this recommendation [9].

6. Consider effects introduced by ion collection at the base of the gap volume when selecting a Faraday probe design. A ceramic base is recommended for investigations at variable or high background pressure [9].

The guidelines provide a framework for determination of on-orbit current density profiles and minimize experimental measurement uncertainty. The recommendations are expected to increase accuracy of total ion beam current to $\pm 3\%$ and increase accuracy of the axial component of ion beam current to $\pm 5\%$. Ideally, the experimental current density profiles extrapolated to vacuum will enable comparison of ground-based measurements with numerical simulations in the absence of facility effects, thereby reducing the computational complexity and time.

Near-field measurements would seem to minimize the uncertainty associated with far-field measurements. However, these measurements introduce new challenges, including probe – induced perturbation of the plasma discharge, a wider range of Debye length in the measurement domain, gradients in the potential field structure, and possibly SEE effects from the probe collector. In addition, ingestion and near-field CEX collisions with facility neutrals are expected to affect near-field measurements. Thus, the ion current density profiles should still be characterized for variations in distance and background pressure. A second set of spatial corrections for measurement geometry may also be necessary to reduce systematic error associated with cylindrical integration as distance from the exit plane increases.

IV. SUMMARY AND CONCLUSIONS

A comprehensive investigation of nude Faraday probe design and analysis techniques was conducted with a nested Faraday probe. Facility effects were studied over a range of downstream measurement distances and background pressures for all probe configurations. Correction factors accounting for variations in distance and angle of the Faraday probe collector surface to the ion beam were introduced through a theoretical analysis with the Hall thruster modeled as two point sources. These correction factors and methods for evaluating plume properties minimized systematic measurement error and facility effects on current density distributions. The corrected plume properties are in line with expected values of ion beam current based on Hall thruster performance and discharge properties [25]. Precision in total ion beam current measurements was within a 3% range for all nested Faraday probe configurations at all distances.

The influence of facility effects on ion migration was isolated and compared to plume expansion of the extrapolated vacuum current density profiles. This approach enabled a more accurate description of the on-orbit current density profiles using ground measurements. Variations in the ion current density with facility background pressure were studied as the superposition of two Gaussian curves. These curves provided qualitative information about the ionization of ingested neutrals and CEX collisions of facility neutrals in the near-field plume. The ratio of the axial component of ion beam current with respect to the total ion beam current was extrapolated with a 2nd order polynomial to the thruster exit plane. Coefficients of the 2nd order polynomial fit varied with background pressure, thruster discharge voltage, and mass flow rate. This extrapolation resulted in consistent agreement to within 1% for all background pressures and probe configurations, and led to a more accurate evaluation of plume divergence

losses in thruster efficiency. For the low-power Hall thruster ion source in this investigation, the axial component of ion beam current at vacuum conditions decreased by approximately 5% to 10% from the exit plane to the far-field plume. This was attributed to CEX collisions with thruster neutrals and divergence by the external potential field structure. Therefore, accurate assessment of the loss in thrust due to ion beam divergence requires ion beam characterization with variations in downstream distance and facility background pressure.

ACKNOWLEDGEMENTS

REFERENCES

[1] D. H. Manzella, J. M. Sankovic, AIAA Paper No. AIAA-95-2927 (1995) (unpublished).

[2] M. L. R. Walker, R. R. Hofer, A. D. Gallimore, J. Propul. Power **22**, 205 (2006).

[3] K. H. de Grys, D. L. Tilley, R. S. Aadland, AIAA Paper No. AIAA-99-2283 (1999) (unpublished).

[4] R. R. Hofer, M. L. R. Walker, A. D. Gallimore, A. D., AIAA Paper No. IEPC-01-020 (2001) (unpublished).

[5] J. L. Rovey, M. L. R. Walker, A. D. Gallimore, P. Y. Peterson, Rev. Sci. Instrum. **77**, 013503 (2006).

[6] M. L. R. Walker, A. L. Victor, R. R. Hofer, A. D. Gallimore, J. Propul. Power **21**, 408 (2005).

[7] J. J. Boerner, Ph.D. dissertation, University of Michigan, 2008.

[8] Y. Azziz, Ph.D. dissertation, Massachusetts Institute of Technology, 2007.

[9] D. L. Brown, A. D. Gallimore, Rev. Sci. Instrum. (Part 1, submitted 2010).

[10] MKS Instruments, Bulletin 01/08 – Series 943 Cold Cathode, February 24, 2010 <http://www.mksinst.com/docs/UR/943DS.pdf>

[11] M. L. R. Walker, A. D. Gallimore, Rev. Sci. Instrum. **76**, 053509 (2005).

[12] P. A. Redhead, Vacuum **38**, 901 (1988).

[13] R. N. Peacock, N. T. Peacock, D. S. Hauschulz, J. Vac. Sci. Technol. A **9**, 1977 (1991).

[14] D. L. Brown, C. W. Larson, B. E. Beal, A. D. Gallimore, J. Propul. Power **25**, 1163 (2009).

[15] L. Brieda, J. Pierru, R. Kafafy, J. Wang, AIAA Paper No. AIAA-2004-3633 (2004) (unpublished).

[16] J. M. Fife, M. R. Gibbons, W. A. Hargus Jr., D. B. VanGilder, D. E. Kirtley, L. K. Johnson, AIAA Paper No. AIAA-2002-4267 (2002) (unpublished).

[17] M. R. Gibbons, D. E. Kirtley, D. B. VanGilder, J. M. Fife, AIAA Paper No. AIAA-2003-4872 (2003) (unpublished).

[18] C. K. Birdsall, IEEE Trans. Plasma Sci. **19**, 65 (1991).

[19] G. A. Bird, *Molecular Gas Dynamics and the Direct Simulation of Gas Flows* (Oxford University Press, Oxford, 2003).

[20] R. L. Spicer, Masters' thesis, Virginia Polytechnic Institute and State University, 2008.

[21] R. R. Hofer, I. Katz, I. G. Mikellides, D. M. Goebel, K. K. Jameson, R. M. Sullivan, L. K. Johnson, K., AIAA Paper No. AIAA-2008-4924 (2008) (unpublished).

[22] C. K. Birdsall, A. Langdon, *Plasma Physics Via Computer Simulations* (Institute of Physics Pub., Philadelphia, 2000).

[23] F. I. Parra, E. Ahedo, J. M. Fife, M. Martinez-Sanchez, J. of Appl. Phys. **100**, 023304 (2006).

[24] B. M. Reid, Ph.D. dissertation, University of Michigan, 2008.

[25] D. L. Brown, Ph.D. dissertation, University of Michigan, 2009.